INDEX COPERNICUS INTERNATIONAL

Bio-Algorithms and Med-Systems

WWW.BAMSJOURNAL.COM ISSN: 1896-530X

Cross sections and gamma yields in (*p*, *x*) reactions on ^{14}N and ^{16}O for ^{14,15}O production

Ihor Kadenko[1,2] (ORCID: 0000-0001-8766-4229), Nadiia V. Sakhno[1,2] (ORCID: 0000-0002-4138-8633), Pawel Moskal[3,4] (ORCID: 0000-0002-4229-3548)

[1]International Nuclear Safety Center of Ukraine of Taras Shevchenko National University of Kyiv, Kyiv, Ukraine
[2]Department of Nuclear and High-Energy Physics, Faculty of Physics, Taras Shevchenko National University of Kyiv, Kyiv, Ukraine
[3]Faculty of Physics, Astronomy and Applied Computer Science, Jagiellonian University, Krakow, Poland
[4]Center for Theranostics, Jagiellonian University, Krakow, Poland

ABSTRACT

Dose delivery in proton beam therapy requires significant effort for in vivo verification. PET is considered as one of the most precise methods for such verification using short-lived radionuclides. One of the newer approaches in proton therapy is based on FLASH therapy, when a 40–60-Gy absorbed dose could be delivered in millisecond time intervals. For this very promising type of therapy a very important task is to reliably identify the beam stopping position within the corresponding organ with a tumor in the patient's body. This could be done if the beam proton energy in the body is still above the threshold of the corresponding nuclear reaction, in the outgoing channel of which will be produced positron-emitting nuclei. In this work we consider the production of oxygen radionuclides emitting positrons ^{14}O (the half-life 70.6 s) and ^{1}O (the half-life 122.2 s). Using the TALYS code, we calculated cross sections of proton-induced nuclear reactions on ^{14}N and ^{16}O, leading to the formation of ^{14,15}O with the application of a well-working optical model. In addition, we calculated total gamma-production and average gamma-emission energy for incident proton energy 150 MeV.

KEYWORDS

oxygen isotopes, proton beam, proton-induced nuclear reactions, cross sections, total-body PET, PET, proton beam therapy

ORIGINAL ARTICLE

Received: 12.12.2023
Accepted: 28.12.2023
Published: 31.12.2023

CITE THIS ARTICLE AS:
Kadenko I, Sakhno NV, Moskal P, "Cross sections and gamma yields in (p, x) reactions on 14N and 16O for 14, 15O production," BAMS vol. 1, no. 1, pp. 140-144, 2023, DOI: 10.5604/01.3001.0054.1974

AUTHORS' CONTRIBUTION:
A – Study Design
B – Data Collection
C – Statistical Analysis
D – Manuscript Preparation
E – Literature Search
F – Funds Collection

CORRESPONDING AUTHOR:
Prof. Ihor Kadenko; International Nuclear Safety Center of Ukraine of Taras Shevchenko National University of Kyiv, Kyiv, Ukraine; Volodymyrska St. 64/13, Kyiv 01601, Ukraine; Phone +38 044 239 3380; E-mail: imkadenko@univ.kiev.ua

INTRODUCTION

Dose delivery in proton beam therapy requires significant effort for its in vivo verification [1]. PET is considered as one of the methods for such verification by using short-lived radionuclides. One of the newer approaches in proton therapy is based on FLASH irradiation, when a 40–60 Gy-absorbed dose could be delivered in millisecond time intervals [2, 3]. The first FLASH beam monitoring tests with novel PET prototypes were recently reported [4–7]. For this very promising type of therapy a very important task is to reliably identify the beam stopping position within the corresponding organ affected by a tumor. This could be done with PET if the beam proton energy in the body is still above the threshold of the corresponding nuclear reaction, in the outgoing channel of which will be produced positron-emitting nuclei [1, 8]. For this purpose one could use oxygen isotopes ^{14}O (half-life, 70.6 s) and ^{15}O (half-life, 122.2 s) as recently demonstrated in [9]. The experimental knowledge of cross-section production for ^{14}O is rather poor. Therefore, we calculated the cross sections of proton-induced nuclear reactions on ^{14}N and ^{16}O, leading to the formation of ^{14,15}O with application of the TALYS-1.96 code [10] using the two-component exciton model to describe preequilibrium processes, and the equilibrium state by the Hauser-Feshbach model. In addition, we calculated total gamma production and average gamma-emission energy for the incident proton energy of 150 MeV.

It is worth noting that an additional generation of ^{14}O in the ^{14}N (*p*, *n*) nuclear reaction "feeds" the tumor cells with more oxygen and makes them more susceptible to damage by protons. The estimation of the production cross section in proton-induced reactions is also important for the development of positronium imaging during proton therapy, which can in principle help in estimating the degree of tissue hypoxia [11–14].

REACTIONS

In our study we considered only proton-induced reactions on main chemical elements of the human body: nitrogen and oxygen, in particular their most abundant isotopes: ^{14}N and ^{16}O, with the formation of ^{14}O and ^{15}O in the output channels. The isotope ^{14}O possess a half-life of 70.6 s and only decays via the EC+β^+ mode. The isotope ^{15}O possess a half-life of 122.2 s and also only decays via the EC+β^+ mode.

A proton-induced reaction on ^{14}N with the production of ^{14}O in the output channel

The kinematic data for the reaction ^{14}N (*p*, *n*)^{14}O is presented below [15] (Tab. I.):

Tab. I. The kinematic data for the reaction ^{14}N (*p*, *n*)^{14}O.

REACTION PRODUCTS	Q-VALUE (KEV)		THRESHOLD (KEV)	Δ, KEV
^{14}O + *n*	–5926.71	3	6353.38	3

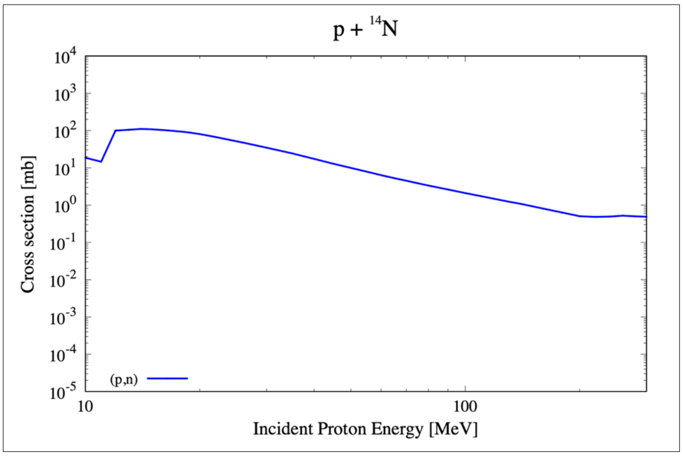

Fig. 1. Calculation results for the ^{14}N (*p*, *n*) ^{14}O nuclear reaction.

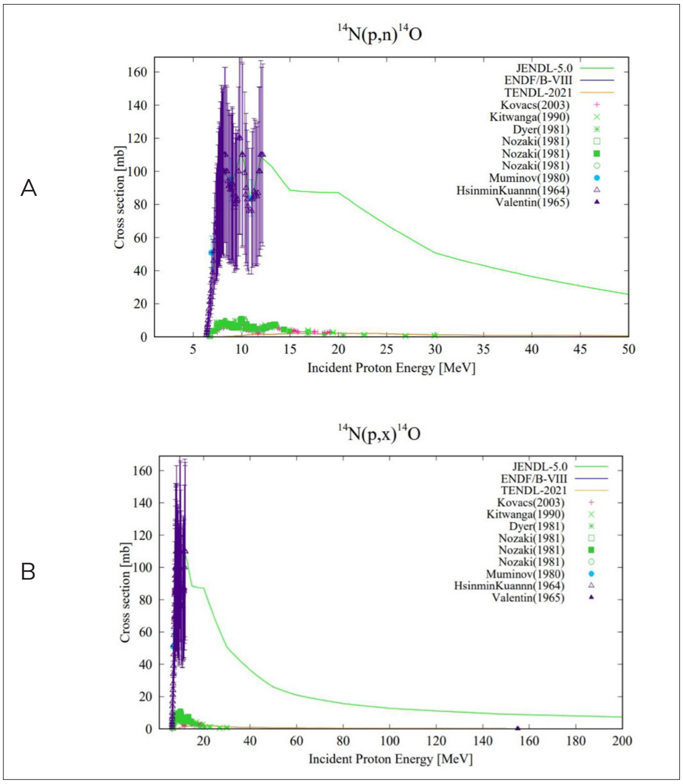

Fig. 2. Experimental, evaluation and calculation results for ^{14}N (*p*, *n*); ^{14}O nuclear reaction for [0 ÷ 50] (A) and [0 ÷ 200] (B) MeV.

The graphic representation of calculation results is shown in Fig. 1. Also, in Fig. 2. one can see the whole picture for this nuclear reaction within the energy range from 10 to 150 MeV. As we note, cross-section reach ~ 100 mb maximum between 10 and 15 MeV drops down to 0.5 mb for proton energies above 120 MeV. In Fig. 2. data are presented from EXFOR [16], JENDL-5.0 [17] and ENDF/B-VIII libraries [18], as well as TALYS [10] calculations. As we can see, JENDL data is very different from TALYS predictions, starting from 12 MeV and on for greater energies. Similar results are for proton-energies below 12 MeV.

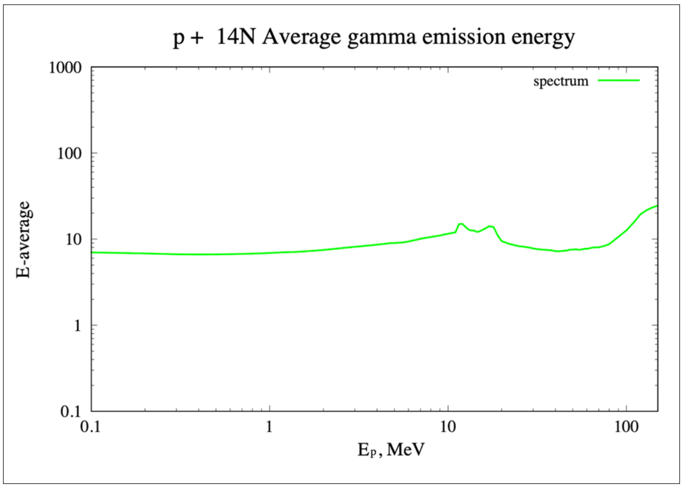

Fig. 3. Average gamma-emission energy generated in the ^{14}N (p, n) ^{14}O nuclear reaction *versus* incident proton energy.

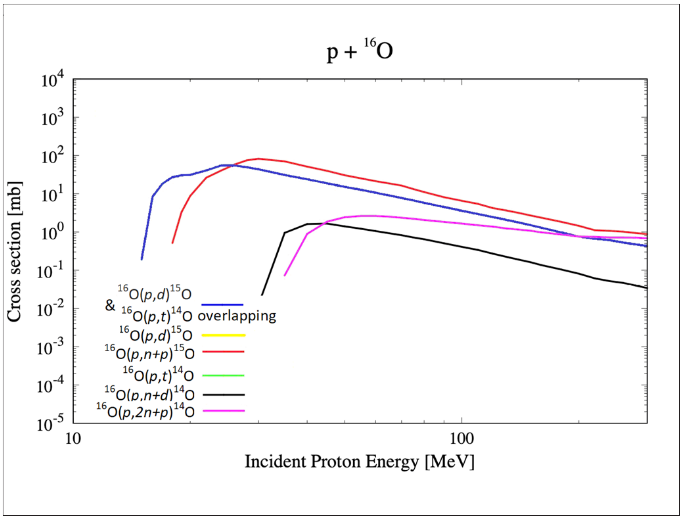

Fig. 4. Cross-section calculation results for the ^{16}O (p, x) $^{14,15}O$ nuclear reactions.

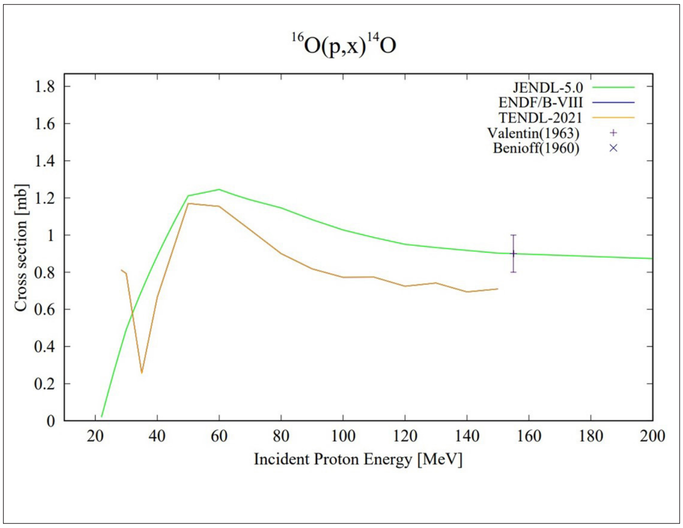

Fig. 5. Experimental, evaluation and calculation results for ^{16}O (p, x) ^{14}O nuclear reaction for [0 ÷ 200] MeV energy range.

Tab. II. The kinematic data for 150 MeV proton energy of incident protons of the ^{16}O (p, x) ^{14}O reactions.

REACTION PRODUCTS	Q-VALUE (KEV)		THRESHOLD (KEV)	Δ, KEV
^{14}O + t	−20405.62	3	21691.79	3
^{14}O + n + d	−26662.85	3	28343.41	3
^{14}O + 2n + p	−28887.42	3	30708.19	3

Tab. III. The kinematic data for the 150 MeV proton energy of incident protons of the ^{16}O (p, x) ^{15}O reactions.

REACTION PRODUCTS	Q-VALUE (KEV)		THRESHOLD (KEV)	Δ, KEV
^{15}O + d	−13439.4	5	14286.5	5
^{15}O + n + p	−15663.9	5	16651.2	5

In addition, it would be of some interest to know the value of the average gamma-emission energy, presented in Fig. 3.

Proton-induced reactions on ^{16}O with the production of ^{14}O in the output channel

The kinematic data for 150 MeV proton energy of incident protons of the ^{16}O (p, x) ^{14}O reactions is presented below (Tab. II.).

The production of ^{14}O takes place in ^{16}O (p, t); ^{16}O (p, *nd*) and ^{16}O (p, 2*np*) nuclear reactions were investigated up to 150 MeV of proton impinging energy. The graphic representation of calculation results shown in Fig. 4. is based on the TALYS-1.96 code. As we can see, for our energy region of interest, (p, t) reaction dominates in the production of ^{14}O and reaches the maximum value of their cross-sections ~ 100 mb at about 25–30 MeV proton energies. The other two reactions, (p, *nd*) and (p, 2*np*), are less likely to occur, and their cross sections are several times less up to the proton energy of 110 MeV, when cross sections of ^{16}O (p, t) and ^{16}O (p, 2*np*) become comparable. Cross sections for the reactions ^{16}O (p, d) ^{15}O (yellow) and ^{16}O (p, t) ^{14}O (green) are overlapping, and both dependencies are presented in blue.

Fig. 5. also presents the whole picture for these nuclear reactions. Data are taken from the EXFOR [16], JENDL-5.0 [17] and ENDF/B-VIII libraries [18], as well as TALYS [10] calculations. As we can see, JENDL data are not very different from TALYS predictions and ENDF/B-VIII, which are practically the same. Very scarce experimental data are available in the EXFOR library.

Proton-induced reaction on ^{16}O with the production of ^{15}O in the output channel

The kinematic data for the 150 MeV proton energy of incident protons of the ^{16}O (p, x)^{15}O reactions is presented below (Tab. III.).

The production of ^{15}O takes place in ^{16}O (p, d) and ^{16}O (p, *np*) nuclear reactions and was investigated up to 150 MeV of proton

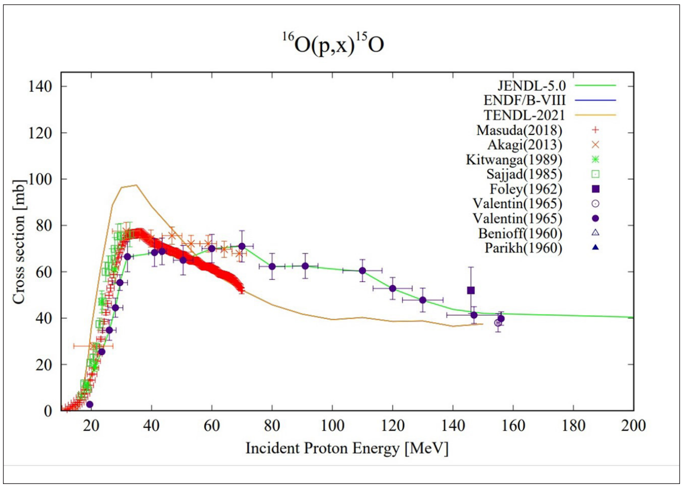

Fig. 6. Experimental, evaluation and calculation results for a ^{16}O (p, x) ^{15}O nuclear reaction for the [0 ÷ 200] MeV energy range.

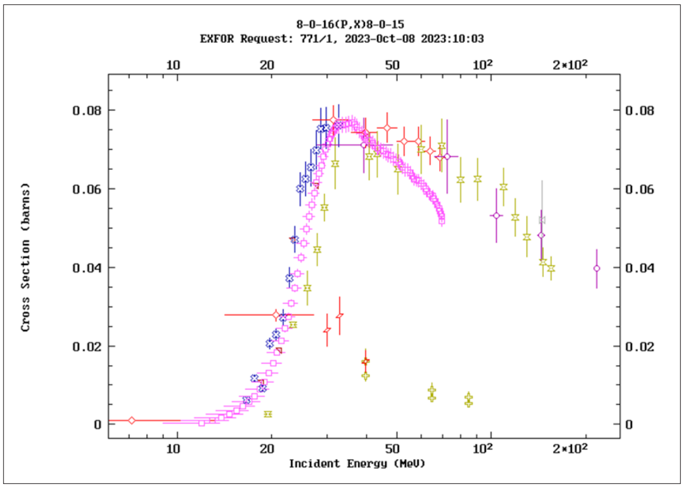

Fig. 7. Up-to-date experimental ^{16}O (p, x) ^{15}O nuclear reaction for a [0 ÷ 200] MeV energy range.

impinging energy. The graphical representation of calculation results is shown in Fig. 4. above. As we can see, for our energy region of interest, (*p*, *np*) and (*p*, *d*) reactions equally dominate the production of ^{15}O, reaching the maximum value of their cross--sections ~ 100 mb at about 25–30 MeV proton energies. As we can see from Fig. 6., much experimental data is available, which creates a solid basis for the theoretical descriptions. Therefore, there is a good correspondence between experimental, evaluated and calculated data. In addition, Fig. 7. depicts the up-to-date experimental data taken from the EXFOR library [16] for 2023.

CONCLUSIONS

In this study the production cross section of ^{14,15}O isotopes in (*p*, *x*) nuclear reactions on ^{14}N and ^{16}O for 150 MeV protons have been calculated using the TALYS-1.96 code via equilibrium and preequilibrium models. Considering the reactions examined in this study, for the production of ^{15}O nuclear data (word missing) are in good agreement among calculations, evaluations and experiments. Data for the production of the ^{14}O isotope is very poor and one can rely only on calculations and evaluations on both isotopes, ^{14}N and ^{16}O. An interesting fact is that the cross--section dependences for ^{16}O (p, t), ^{14}O and ^{16}O (p, d) ^{15}O nuclear reactions are nearly identical.

ACKNOWLEDGMENT

This work was supported by the Foundation for Polish Science through the TEAM POIR.04.04.00-00-4204/17 program and the SciMat and qLife Priority Research Area budget under the auspices of the program Excellence Initiative – Research University at Jagiellonian University.

REFERENCES

1. Parodi K, Yamaya T, Moskal P. Experience and new prospects of PET imaging for ion beam therapy monitoring. Z Med Phys. 2023;33:22-34. doi: 10.1016/j.zemedi.2022.11.001.
2. Graeff C, Volz L, Durante M. Emerging technologies for cancer therapy using accelerated particles. Prog Part Nucl Phys. 2023;131:104046. doi: 10.1016/j.ppnp.2023.104046.
3. Durante M, Orecchia R, Loeffler JS. Charged-particle therapy in cancer: clinical uses and future perspectives. Nat Rev Clin Oncol. 2017;14(8):483-95. doi: 10.1038/nrclinonc.2017.30.
4. Lang K. Towards high sensitivity and high resolution PET scanners: imaging--guided proton therapy and total body imaging. BAMS. 2022;18:96-106. doi: 10.2478/bioal-2022-0079.
5. Abouzahr F, Cesar JP, Crespo P, Gajda M, Hu Z, Kaye W, et al. The first PET glimpse of a proton FLASH beam. Phys Med Biol. 2023;68:125001. doi: 10.1088/1361-6560/acd29e.
6. Abouzahr F, Cesar JP, Crespo P, Gajda M, Hu Z, Klein K, et al. The first probe of a FLASH proton beam by PET. Phys Med Biol. 2023;68:235004. doi: 10.1088/1361-6560/ad0901.
7. Jäkel O. Physical advantages of particles: protons and light ions. Br J Radiol. 2020;93:20190428. doi: 10.1259/bjr.20190428.
8. Brzeziński K, Baran J, Borys D, Gajewski J, Chug N, Coussat A, et al. Detection of range shifts in proton beam therapy using the J-PET scanner: a patient simulation study. Phys Med Biol. 2023;68:145016. doi: 10.1088/1361-6560/acdd4c.
9. Purushothaman S, Kostyleva D, Dendooven P, Haettner E, Geissel H, Schuy C, et al. Quasi-real-time range monitoring by in-beam PET: a case for 15O. Sci Rep. 2023; 13(1):18788. doi: 10.1038/s41598-023-45122-2.
10. Koning AJ, Rochman D, Sublet JC, Dzysiuk N, Fleming M, van der Marck S. TENDL: Complete Nuclear Data Library for Innovative Nuclear Science and Technology. Nucl Data Sheets. 2019;155:1-55.
11. Moskal P, Dulski K, Chug N, Curceanu C, Czerwiński E, Dadgar M, et al. Positronium imaging with the novel multiphoton PET scanner. Sci Adv. 2021;7:eabh4394. doi: 10.1126/sciadv.abh4394.

12. Bass SD, Mariazzi S, Moskal P, Stępień E. Colloquium: Positronium physics and biomedical applications. Rev Mod Phys. 2023;95:021002. doi: 10.1103/RevModPhys.95.021002.
13. Moskal P, Stępień EŁ. Positronium as a biomarker of hypoxia. Bio-Algorithms and Med-Systems. 2021;17(4):311-9. doi: 10.1515/bams-2021-0189.
14. Shibuya K, Saito H, Nishikido F, Takahashi M, Yamaya T. Oxygen sensing ability of positronium atom for tumor hypoxia imaging. Commun Phys. 2020;3:173. doi: 10.1038/s42005-020-00440-z.
15. National Nuclear Data Center [Internet]. Q-Value Calculator (QCalc) [cited 2023 Dec 12]. Available from: https://www.nndc.bnl.gov/qcalc.
16. Experimental Nuclear Reaction Data (EXFOR) [cited 2023 Dec 12]. Available from: https://www-nds.iaea.org/exfor.
17. JAEA Nuclear Data Center [Internet]. JENDL-5 [cited 2023 Dec 12]. Available from: https://wwwndc.jaea.go.jp/jendl/j5/j5.html.
18. National Nuclear Data Center [Internet]. ENDF/B-VIII.0 Evaluated Nuclear Data Library [cited 2023 Dec 12]. Available from: https://www.nndc.bnl.gov/endf-b8.0.